

PHYSICAL REVIEW C

NUCLEAR PHYSICS

THIRD SERIES, VOLUME 31, NUMBER 2

FEBRUARY 1985

Neutron-proton radiative capture cross section at $T_n = 185$ MeV

H. O. Meyer, J. R. Hall, M. Hugi, H. J. Karwowski, R. E. Pollock, and P. Schwandt

Indiana University Cyclotron Facility, Bloomington, Indiana 47405

(Received 24 September 1984)

The differential cross section for the reaction $p(n,d)\gamma$ has been measured for center-of-mass angles between 0° and 65° at a neutron kinetic energy $T_n = 185$ MeV. Assuming time-reversal invariance, our result is in essential agreement with the deuteron photodisintegration measurement at $\theta_p = 0^\circ$ performed by Hughes *et al.* at Mainz. In addition to this confirmation of the absolute magnitude, our results, for the first time, provide information on the shape of the cross section distribution near 0° , i.e., the region where existing theories show the largest differences. This paper contains a detailed account of the experiment and a comparison with relevant experimental information. A discussion of some theoretical implications is also included. The best agreement with our data is obtained from these theories where relativistic corrections to the charge density are taken into account.

I. INTRODUCTION

Photodisintegration of the deuteron was first observed by Chadwick and Goldhaber¹ fifty years ago. Soon thereafter Bethe and Peierls² investigated the theoretical aspects of electromagnetic transitions in the $n + p$ system. Breit and Condon³ pointed out the importance of deuteron photodisintegration as a source of information on the nucleon-nucleon (NN) force. Early theoretical efforts thus focused on various aspects of the NN potential. The first three decades of refining the theory of NN radiative transitions culminated in Partovi's well-known, nonrelativistic impulse approximation calculation⁴ of deuteron photodisintegration observables at photon energies from 10 to 140 MeV.

Partovi's calculation was in general agreement with the experimental data available at that time (cf. references listed in Ref. 4). However, these early experiments were beset by systematic errors such that some of the results at overlapping angles and energies are clearly inconsistent with each other. A significant improvement in the quality of photodisintegration data was achieved by Weissmann and Schultz⁵ who published ${}^2\text{H}(\gamma,p)n$ cross sections for E_γ from 27 to 55 MeV. These measurements were the first to show quantitative disagreement with Partovi's results. The existence of serious difficulties became clear following a careful measurement⁶ at the Mainz linac of the $\theta = 0^\circ$ cross section for deuteron photodisintegration over the energy range $20 \text{ MeV} < E_\gamma < 120 \text{ MeV}$. An excellent review of the field of neutron-proton radiative transitions prior to 1979 was given by Firk.⁷

Discrepancies between theory and experiment in a process as basic as the radiative transition in the NN system are disturbing, and a number of attempts to reconcile the

theory with the data were initiated as a consequence. In parallel, it became clearly necessary to verify the experimental findings: At the lower end of the energy range covered by the Mainz group⁶ their photodisintegration results were confirmed by a cross section measurement⁸ at $\theta = 0^\circ$ of the radiative capture process ${}^1\text{H}(n,d)\gamma$ for $T_n = 72$ MeV. The two cross sections are related by detailed balance if time reversal invariance is assumed.

In this paper we present a measurement of the absolute cross section for the neutron-proton radiative capture reaction ${}^1\text{H}(n,d)\gamma$ at a neutron bombarding energy of $T_n = 185 \text{ MeV} \pm 5 \text{ MeV}$. The results have been obtained with an experimental geometry which not only covered the angular region around $\theta = 0^\circ$ but also extended continuously to $\theta = 65^\circ$ in the center-of-mass system, providing new information on the *shape* of the differential cross section as well as the absolute magnitude. Neutron-proton elastic scattering was observed simultaneously and was used to normalize the measurements. This greatly reduces many of the possible systematic uncertainties. A preliminary account of this experiment has recently appeared in print.⁹

In Sec. II we describe the experimental procedure. A discussion of our results and a comparison with other experiments is contained in Sec. III. The consequences of this measurement with respect to various theoretical approaches are outlined in Sec. IV followed by conclusions in Sec. V.

II. EXPERIMENTAL PROCEDURE

A. Measurement

A view of the experimental apparatus is shown in Fig. 1; in the following, curly braces refer to labels mentioned

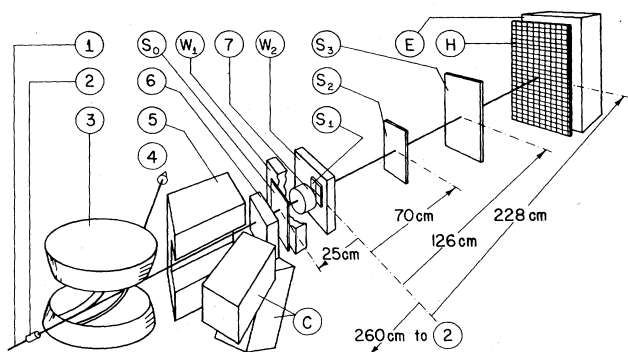


FIG. 1. Schematic view of the experimental apparatus. The labels are referred to in the text.

in this figure. The experiment has been carried out at the Indiana University Cyclotron Facility in the so-called beam swinger area which, after some modification, served as an intense neutron source. Neutrons were produced by means of the ${}^7\text{Li}(p,n)$ reaction to the ground state and first excited state of ${}^7\text{Be}$. The production target {2} consisted of 2.1 g/cm^2 natural lithium covered with a 1 mg/cm^2 protective layer of nickel. The incident proton beam {1} of 191.1 MeV kinetic energy was limited in intensity to about 40 nA by the onset of count rate instability in some of the detectors. After passage through the Li target the proton beam was deflected {3} and its current was integrated in a Faraday cup {4}.

The resulting neutron beam, now in air, passed through a $10\times 10\text{ cm}$ lead collimator {5} and a 5 cm thick lead absorber {6} designed to stop remaining charged particles. At a distance of 260 cm from the production target a typical neutron flux of $3\times 10^4\text{ s}^{-1}\text{ cm}^{-2}$ was obtained.

The proton target {7} consisted of liquid hydrogen in a thin-walled, cylindrical stainless steel container 11.2 cm in diameter and 6.4 cm thick. The flat end caps exposed to the neutron beam were made of 20 mg/cm^2 stainless steel. This container could be filled with liquid hydrogen by using a commercial expansion refrigerator attached to a helium compressor to condense hydrogen gas from a storage volume into the target vessel. In the filling process all condensible impurities were removed from the gas. After use, the target material was checked for impurities by mass spectroscopic analysis. The method of temperature stabilization, performance characteristics, and safety precautions taken when operating the liquid hydrogen target are described elsewhere.¹⁰

A scintillator $\{S_0\}$, $3.4\times 152\times 152\text{ mm}$, vetoed charged particles that were generated by the neutron beam in the Pb absorber before they entered the target. Protons and deuterons produced in the target were detected by an array of plastic scintillator detectors. The first, $\{S_1\}$, with four separate elements of $1.3\times 19.7\times 19.7\text{ mm}$ each, provided the reference time and part of the angle definition for the outgoing particles. The purpose of $\{S_2\}$, $1.8\times 152\times 203\text{ mm}$, and $\{S_3\}$, $1.7\times 229\times 343\text{ mm}$, was to reduce, by imposing additional coincidence requirements, the fraction of accidental events, which otherwise would be a problem in the presence of high singles count

rates, caused by reactions in the scintillators induced by the passing neutron beam. Directional information was provided by a scintillator hodoscope $\{H\}$, consisting of 15×23 cells of $20\times 20\text{ mm}$ each, in conjunction with the segmented detector $\{S_1\}$; the distances between detectors are given in Fig. 1. The geometrical angular resolution limit set by the hodoscope cell size was $\pm 0.3^\circ$. The kinetic energies of the observed charged particles were measured by a thick plastic scintillator $\{E\}$, $51\times 326\times 505\text{ mm}$, immediately following the hodoscope. The thickness of the H_2 target and of $\{S_1\}$, $\{S_2\}$, and $\{S_3\}$ was chosen to limit angular broadening by multiple scattering to less than the geometrical angular resolution. In order to minimize dependence of the signal on event position, light guides with photomultipliers were attached to both the top and bottom of the $\{S_2\}$, $\{S_3\}$, and $\{E\}$ detectors. A special base circuit was developed to stabilize the voltage at the last three dynodes of the photomultipliers in order to ensure constant amplitude response in the presence of rates up to 0.5 MHz .

The hodoscope employed a double layer of partly overlapping strips of 3.2 mm thick scintillator in both the vertical and horizontal directions. Thus, the coincidence level of the event was part of the position information and the matrix of 15×23 cells could be covered by 20 photomultiplier signals. A comparison of events in cells with one or two layers of scintillator showed that a correction for accidental events in the hodoscope was negligible.

The active target volume was defined longitudinally by the detectors $\{S_0\}$ and $\{S_1\}$ and laterally by the overlap cone of $\{S_1\}$ and $\{E\}$. It contained material other than hydrogen that could give rise to deuterons that could not be distinguished from those from the $p(n,d)\gamma$ reaction. Most of these background events stemmed from the ${}^{12}\text{C}(n,d){}^{11}\text{B}$ reaction in the downstream and upstream layers of $\{S_0\}$ and $\{S_1\}$, respectively (the effective thickness of these layers was determined by the discriminator thresholds). In order to alleviate this problem, two wire chambers $\{W_1\}$ and $\{W_2\}$ were used to better define the target zone. These chambers featured a time resolution of better than 10 ns and presented only little mass to the beam, thus effectively reducing the background. Each of the two chambers consisted of a $10\times 10\text{ cm}$ wire plane halfway between graphite-coated Mylar cathode planes, 12.8 mm apart. Gold-plated tungsten wires with a diameter of $20\text{ }\mu\text{m}$ and 2.0 mm spacing were used. The chambers were housed in gas-tight enclosures forming part of the liquid hydrogen Dewar. A mixture of argon, isobutane, and bromotrifluoromethane, saturated with dimethoxymethane at 273 K , constituted the chamber gas. Thus, the only material in the target zone, other than hydrogen, was four layers of 20 mg/cm^2 stainless steel, two for the target cell and two for the vacuum enclosure. The material for the cell windows was chosen after a comparative study of the (n,d) production cross section for deuterons comparable in energy with those from the $p(n,d)\gamma$ process. For foils of equal tensile strength this cross section was found, for example, to be six times smaller for steel than for Mylar.

For diagnostic purposes, two rectangular lead glass Čerenkov detectors $\{C\}$, $15\times 15\times 30\text{ cm}$, were mounted

such that gamma rays from the $p(n,d)\gamma$ reaction, if detected in coincidence, corresponded kinematically to deuterons in specific regions of the hodoscope $\{H\}$. A sample of such well-defined, background-free capture events provided useful diagnostic information in checking important aspects of the data analysis. However, in view of uncertainties in effective aperture and gamma detection efficiency of the Čerenkov detectors, no use was made of the capture photons in determining the final cross section values.

A relative measurement of the neutron flux was derived from the counting rate in a 25 mm thick scintillator placed downstream of $\{E\}$ (not shown in Fig. 1) which was operated in anticoincidence with $\{E\}$.

Whenever the condition $\{\bar{S}_0\} \cdot \{S_1\} \cdot \{S_2\} \cdot \{S_3\} \cdot \{E\}$ was true, pulse heights and flight times with respect to $\{S_1\}$ for all detectors were stored on magnetic tape. An exception to this event definition was the class of events where the flight time from $\{S_1\}$ to $\{E\}$ was consistent with that of an elastically scattered $p(n,p)n$ proton. Of these frequent events only a random sample of 4.6% was admitted in order to compensate for the large cross section difference between the $p(n,d)\gamma$ and $p(n,p)n$ processes. This sampling fraction was carefully monitored at all times during the experiment. In addition, about 10% of the stored events were generated by a randomly triggered pulser. These pulser events were used to measure the dead time of the apparatus and to investigate the probability with which a random coincidence could lead to an unwanted event. Also continuously monitored during the experiment was the efficiency of both wire chambers by scaling appropriate coincidences between the wire chambers and several of the scintillators in the detector stack. The rate

at which events were written to tape was about 35 s^{-1} , with about 500 bits recorded per event.

Events arising from either of the two processes $p(n,d)\gamma$ or $p(n,p)n$ were selected off line. Those events that either fire $\{W_1\}$, or that do not fire $\{W_2\}$, or that are inconsistent with the velocity of a prompt incident neutron, were eliminated. The neutron velocity was defined by exploiting the subnanosecond IUCF beam burst structure and measuring the elapsed time between the last cyclotron r.f. cycle and the $\{S_1\}$ timing signal. The final result was demonstrated to be insensitive to varying, within reason, the off-line sorting condition imposed on the neutron velocity.

The mass of the reaction products (mainly protons and deuterons) was determined from the time of flight from $\{S_1\}$ to $\{E\}$ and from the energy deposited in the $\{E\}$ detector. Figure 2 displays a sample of prompt neutron events sorted according to these two parameters. The energy region occupied by the elastically scattered protons from $p(n,p)n$ can be readily identified in the left part of the figure. The right-hand side shows the proton locus populated by bremsstrahlung events and by (n,p) reactions in the steel windows together with the less prominent locus containing the deuterons of interest. An additional improvement of the separation between protons and deuterons was achieved by making use of time and energy information from the $\{S_2\}$ and $\{S_3\}$ detectors. The selection condition imposed on deuterons had to encompass all events of interest but still had to be restrictive in order to discriminate against background deuterons as much as possible. Again, the procedure followed has been verified by checking the sensitivity of the final result to variations of the deuteron window condition.

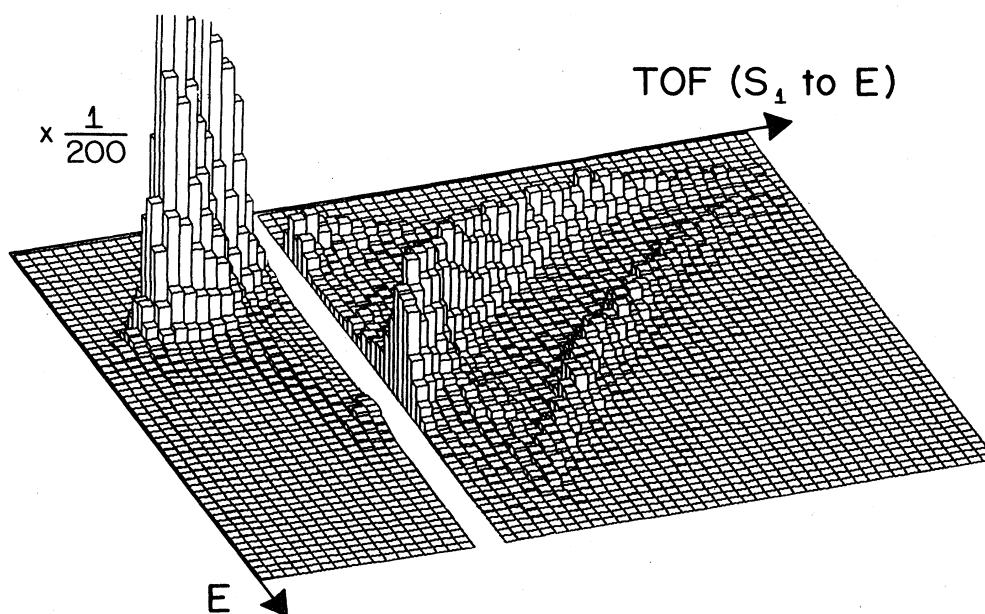


FIG. 2. Time of flight versus energy deposited in $\{E\}$ for a sample of events induced by prompt neutrons. Visible are the peak from elastically scattered protons, the proton locus due to bremsstrahlung events, and the less prominent deuteron locus containing the events of interest. The scale chosen, together with the sampling fraction for elastic events, results in a suppression of a factor of 200 of the left part of the figure. The target-empty background has not been subtracted in this figure.

In order to correct for the presence of background deuterons from (n,d) reactions in the target windows, measurements were made with and without liquid hydrogen in the target cell. The relative normalization between such runs was obtained from the integrated charge of the primary proton beam. Except for a few runs with known deficiencies, using the integrated neutron flux led to the same result. The relative normalizations of runs also contained a contribution from the dead time of the data acquisition system (typically between 2% and 6%) and from the efficiencies of the two wire chambers (typically between 91% and 98%). Strictly, the target-empty measurement yielded a biased measurement of the deuteron background since deuterons originating upstream from the target are degraded in energy when passing through hydrogen. A correction for this effect depends on the energy spectrum of the background deuterons, which in turn was determined from the events collected with the target empty, and was found to agree with a measured spectrum¹¹ for $^{56}\text{Fe}(p,d)^{55}\text{Fe}$ at $T_p = 185$ MeV. The size of this effect turned out to be small and merely led to an additional error of $\pm 2\%$.

The data presented here were collected in 95 separate runs. During an actual data taking time of 85 h a total of 10^6 (sampled) protons from $p(n,p)n$ and 3×10^4 deuterons from $p(n,d)\gamma$ were accumulated. The data accumulation time was divided in the ratio of 5:4 between target full and empty, respectively. After all sorting conditions were applied the ratio of deuterons of interest to background deuterons, averaged over angle, was about 2:1.

B. Data analysis

The reaction angle of every valid event was determined from the response pattern in detector $\{S_1\}$ (4 elements) and the hodoscope $\{H\}$ (345 elements). The finite geometry of the setup and the angular variation of the neutron flux incident on the target were taken into account in a computer simulation to determine the mean reaction angles that correspond to any $\{S_1\}$ - $\{H\}$ element combination. The same computer code was also used to

predict the population by elastically scattered protons for any given pair of elements. From a comparison of this prediction with the actually accumulated proton data the effective $\theta = 0^\circ$ axis of the apparatus was determined. Such a procedure is necessary since the physical axis depends on the direction and distribution of the incident neutron beam.

For each $\{S_1\}$ - $\{H\}$ element combination the ratio of laboratory cross sections

$$R_{dp} = \sigma[p(n,d)\gamma] / \sigma[p(n,p)n]$$

was determined from the corresponding background-corrected numbers of deuterons and protons. Combining these ratios R_{dp} , taking into account the respective reaction angles, finally yielded the actual result of this experiment, namely the *cross section ratio* $R_{dp}(\theta_{lab})$ between $n + p$ radiative capture and $n + p$ elastic scattering. The angular binning chosen ($\delta\theta = \pm 0.35^\circ$) reflects the experimental angular resolution. These results are listed in the first two columns of Table I and displayed in Fig. 3(a).

The errors shown are mainly statistical, but also contain estimated contributions from the background subtraction ($\pm 2\%$) and relative uncertainties in detector efficiencies ($\pm 3\%$). An additional error has also been included for the two largest measured angles to account for the possible loss of deuterons which fall close to the deuteron energy acceptance limit of our experimental arrangement.

The result of the present experiment has been subjected to a number of tests. These include the sensitivity checks on the cuts applied during the off-line sorting, as described earlier. In addition, results from the individual 95 temporal segments of the measurement and from different parts of the hodoscope and the detector $\{S_1\}$ were tested for consistency. Using the randomly triggered pulser events, the contribution of accidental coincidences was assessed and found negligible. By the nature of this experiment, possible systematic effects are only those which affect the outgoing protons and deuterons in a different way. Uncertainties, for example, in the neutron flux, the hydrogen target thickness, and geometrical acceptances, cancel in the determination of $R_{dp}(\theta_{lab})$. Possi-

TABLE I. Measured cross section ratio R_{dp} vs laboratory angle θ_{lab} and quantities derived as described in the text.

θ_{lab} (deg)	R_{dp} (10^{-3})	σ_{lab}^a $^1\text{H}(n,p)n$ (mb/sr)	σ_{lab} $p(n,d)\gamma$ ($\mu\text{b/sr}$)	$\theta_{c.m.}$ (deg)	$\sigma_{c.m.}$ $p(n,d)\gamma$ (nb/sr)	$\sigma_{c.m.}$ $d(\gamma,p)n$ ($\mu\text{b/sr}$)
0.35	0.75 \pm 0.07	49.8 ^b	37.4 \pm 3.7	2.7	649 \pm 64	4.59 \pm 0.45
1.05	0.80 \pm 0.05	49.1	39.4 \pm 2.5	8.0	680 \pm 44	4.81 \pm 0.31
1.75	0.86 \pm 0.05	48.1	41.4 \pm 2.2	13.4	709 \pm 37	5.02 \pm 0.26
2.45	0.92 \pm 0.04	46.9	43.1 \pm 2.0	18.8	729 \pm 34	5.16 \pm 0.24
3.15	1.00 \pm 0.04	45.5	45.4 \pm 2.0	24.4	752 \pm 33	5.32 \pm 0.23
3.85	1.16 \pm 0.05	43.9	50.7 \pm 2.0	30.1	818 \pm 33	5.79 \pm 0.23
4.55	1.19 \pm 0.05	42.1	50.2 \pm 2.1	36.0	782 \pm 33	5.53 \pm 0.23
5.25	1.41 \pm 0.06	40.3	56.7 \pm 2.4	42.2	842 \pm 35	5.96 \pm 0.25
5.95	1.74 \pm 0.08	38.4	67.0 \pm 3.0	48.9	933 \pm 42	6.60 \pm 0.30
6.65	2.07 \pm 0.13	36.4	75.3 \pm 4.6	56.2	957 \pm 59	6.77 \pm 0.42
7.35	2.37 \pm 0.23	34.5	81.5 \pm 7.8	64.4	924 \pm 90	6.54 \pm 0.64

^aSame as the solid curve in Fig. 3.

^bThis value was normalized to published elastic scattering data (see the text).

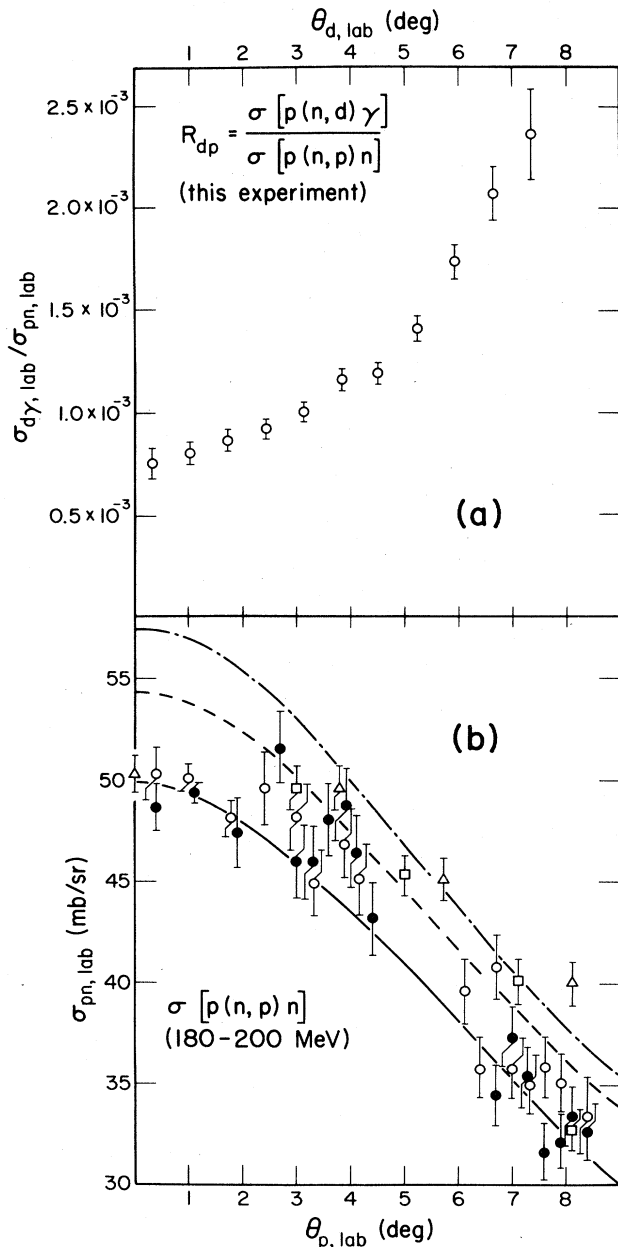


FIG. 3. (a) The cross section ratio $\sigma[p(n,d)\gamma]/\sigma[p(n,p)n]$ which represents the actual result of this experiment. (b) $p(n,p)n$ elastic laboratory cross section near $T_n=180-200$ MeV. The origin of the data is as follows: triangles from Ref. 13, squares from Ref. 12, open and full circles from Ref. 14. The dashed curve is calculated for $T_n=190$ MeV from solution SM84 of a phase shift analysis (Ref. 15), and the dash-dot curve follows from the Paris potential (Ref. 16). The solid curve marks the $p(n,p)n$ cross section assumed for the purpose of normalizing the data of this experiment.

ble systematic effects arising from the difference between protons and deuterons, such as the measurement of the wire chamber efficiencies, the multiple scattering of the outgoing particles, and reaction losses in the scintillators and the air between them, have been estimated and found

to be small compared to the experimental errors quoted previously.

III. RESULTS

A. The cross section for $p(n,d)\gamma$ or $d(\gamma,p)n$

The results of this experiment consist of the measured ratios $R_{dp}(\theta_{lab})$ between the cross sections of $p(n,d)\gamma$ and $p(n,p)n$ as displayed in Fig. 3(a). In order to arrive at the cross section value for $p(n,d)\gamma$ at any θ_{lab} the ratio $R_{dp}(\theta_{lab})$ has to be multiplied by the appropriate elastic scattering cross section. The presently available measurements¹²⁻¹⁴ of the "charge exchange" elastic nucleon-nucleon cross section around 200 MeV over the range of relevant angles are shown in Fig. 3(b) together with solution SM84 of a global phase shift analysis¹⁵ and a calculation¹⁶ derived from the Paris potential.¹⁶ From Fig. 3(b) it is obvious that in this kinematical region commonly accepted parametrizations of the nucleon-nucleon interaction are in substantial disagreement with the data, and that the data themselves are not internally consistent. In view of the fact that our knowledge of this elementary process is clearly inadequate for our purpose, we have *defined*, for the time being, a "most likely" value for $\sigma_{lab}(pn)$, which is shown as a solid curve in Fig. 3(b) and listed in the third column of Table I. This solid curve has been constructed arbitrarily to be similar in shape to the result of the phase shift analysis but in agreement with the *data* at the most forward angles. Note the zero offset in Fig. 3(b). If we chose the phase shift result (dashed line) as a normalization, the $p(n,d)\gamma$ cross section would have shifted upwards by about one standard deviation.

The resulting laboratory cross sections for $p(n,d)\gamma$ are listed in the fourth column of Table I. The rest of Table I contains the data transformed to the center-of-mass system and, by the use of detailed balance, to the frame of the time-reversed deuteron photodisintegration process. In this frame, the photon energy corresponding to $T_n=185$ MeV is $E_\gamma=95$ MeV. The results of this experiment are shown as solid circles in Figs. 5-7, and as a shaded area in Fig. 4.

The $d(\gamma,p)n$ center-of-mass cross section at $\theta=0^\circ$ resulting from this experiment has been obtained by fitting to our data a third-order polynomial in $\cos\theta$ yielding

$$\sigma_{c.m.}[\theta=0^\circ, d(\gamma,p)n]=4.83\pm 0.45 \mu\text{b/sr}.$$

It needs to be emphasized that in this experiment a cross section *ratio* was measured and that the quoted cross sections for the capture process depend on the choice of normalization of the elastic scattering process. Unfortunately, this choice is not unambiguous. One may argue, for instance, that the result of a NN phase shift analysis is superior as a reference since it is based on a large number of data points. We felt, however, that we should not rely on theoretical arguments, even if they are fairly model independent, if measurements exist in the kinematical region in question. To resolve this dilemma absolute cross section measurements of $p(n,p)p$ near 200 MeV are needed. This paper contains sufficient information to calcu-

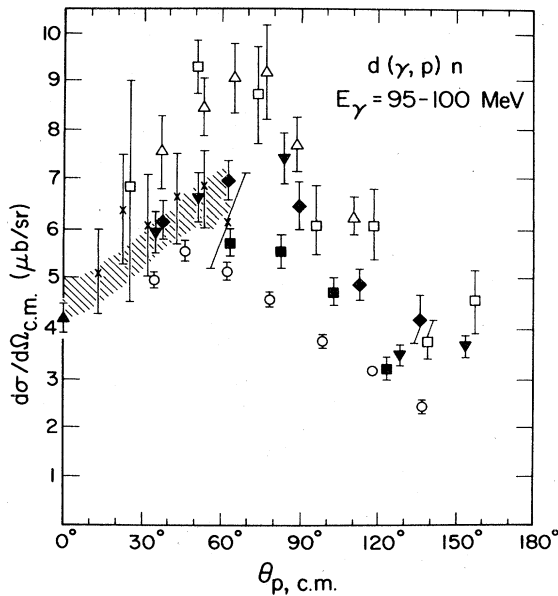


FIG. 4. Comparison of available deuteron photodisintegration cross sections near $E_\gamma=95$ MeV. The data (in chronological order) are from the following laboratories: \blacktriangledown , Urbana (Ref. 17); \blacksquare , Caltech (Ref. 18); \square , Lebedev Institute (Ref. 19); \circ , Bonn (Ref. 20); \blacktriangle , Mainz (Ref. 6); \triangle , Lund (Ref. 21); and \blacklozenge , Frascati (Ref. 22). Also displayed are the radiative capture results from this experiment (shaded region) and from SIN (Ref. 25) (crosses).

late the effect on $p(n,d)\gamma$ of a change in the elastic scattering normalization.

B. Comparison with other experiments

In the past, a number of photodisintegration measurements have been carried out near $E_\gamma=95$ MeV which can be compared to the present experiment. The situation is summarized in Fig. 4, where the results of this experiment are shown as a shaded area. Three early measurements were reported from Illinois¹⁷ (solid triangle, point down), from Caltech¹⁸ (solid squares), and from the Lebedev Institute¹⁹ (open squares). The detection techniques used include, e.g., nuclear emulsions¹⁷ and often seemed crude by today's standards. In a similar experiment from Bonn²⁰ (open circles) the outgoing neutron and proton were detected in coincidence. The Bonn results disagree by up to a factor of 2 with more recent data from Lund²¹ (open triangles). It is clear that there are serious normalization problems with at least one of these experiments. The most recent deuteron photodisintegration data at this energy were obtained at Frascati²² (solid diamonds) and at MIT (Ref. 23) (preliminary, unpublished).

The only data so far obtained by neutron-proton radiative capture at T_n around 200 MeV are from this experiment (shaded region in Fig. 3), from TRIUMF (Ref. 24) (preliminary, unpublished), and from SIN (Ref. 25) (crosses). The SIN measurement has been carried out with rather large, 100 MeV wide bins for the incident neutron energy.

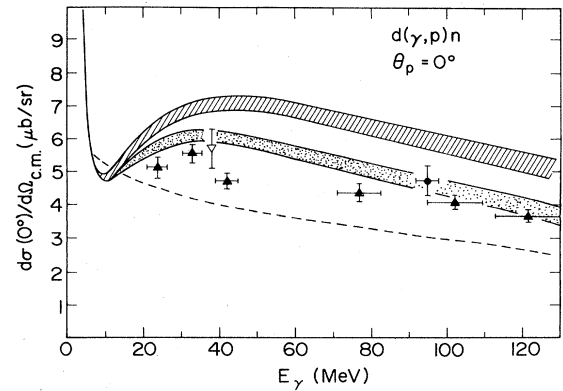


FIG. 5. Center-of-mass differential photodisintegration cross sections at $\theta=0^\circ$. The solid triangles are the photodisintegration data from Mainz (Ref. 6). Radiative capture results are from Louvain (Ref. 8) (open triangle) and from this experiment (solid circle). The shaded band is from Ref. 31 and results from non-relativistic impulse-approximation calculations using eight different NN potentials. If relativistic corrections to the $E1$ operator are included (Ref. 31), the stippled band is obtained. The dashed curve is from Ref. 43.

One finds from Fig. 4 that among those experiments which overlap in angle with our measurement the data from the Lebedev Institute,¹³ Bonn,²⁰ and Lund²¹ are not consistent with the results reported here. These data sets also differ the most from an average of all available data.

Also shown in Fig. 4 is the interpolated result of the original Mainz experiment⁶ (solid triangle, point up). The current experimental situation at $\theta=0^\circ$ is reviewed in Fig. 5, where the results from Mainz⁶ (solid triangles) are compared with the capture result from Louvain⁸ (open triangle) and with the extrapolated cross section at $\theta=0^\circ$ from this experiment (solid circle). The three experiments are, within errors, in agreement with each other.

IV. THEORETICAL IMPLICATIONS

It has been suggested by Barshay²⁶ that the processes $d + \gamma \leftrightarrow n + p$ could represent a case where the invariance under time reversal is violated. The large effect predicted in the Δ resonance region was contradicted by subsequent experiments.²⁷ Since at present any indication of a violation of time reversal invariance in strong and electromagnetic interactions is lacking, we have made use of detailed balance to convert data and calculations to the framework of the $d(\gamma, p)n$ reaction in order to facilitate comparison. In the following we concentrate on those aspects of the theory that are connected with the findings of this experiment and that concern the angular distribution at $E_\gamma=95$ MeV and the $\theta=0^\circ$ excitation function of the cross section for $d(\gamma, p)n$.

It has been suggested for a long time³ that deuteron photodisintegration is a source of information on the NN interaction. It was thus natural to try to explain the discrepancy at $\theta=0^\circ$ by shortcomings of the Hamada-Johnston NN interaction used by Partovi⁴ as phenomenological input. Since the cross section at $\theta=0^\circ$ is especially

sensitive to the D state of the deuteron, it was indeed found that a change in the D -state probability, P_D , of the deuteron can be used to lower the theoretical prediction at will.²⁸ It was soon realized,^{29,30} however, that the required change could not be reconciled with observable properties of the deuteron such as the asymptotic D to S state ratio and the quadrupole moment. In addition, the $\theta=0^\circ$ cross section is not very sensitive to reasonable variations of the NN force, as is illustrated in Fig. 5, where the shaded band contains analogous, nonrelativistic impulse approximation calculations³¹ for eight different NN potentials. An example of the sensitivity of the $d(\gamma,p)n$ cross section to the underlying NN interaction is given in Fig. 6 where Partovi's result⁴ (solid line), which is based on the Hamada-Johnston potential ($P_D=7\%$), is compared with a calculation³² (dotted line) with the same code but with the Lomon-Feshbach NN interaction ($P_D=4.6\%$). The latter calculation has been carried out for $E_\gamma=95$ MeV and, to our knowledge, is the best representation of our data in a classical framework. The sensitivity of radiative neutron-proton capture to the NN potential at short and intermediate range also has been discussed on general grounds (using unitary phase-equivalent transformations) by Greben and Woloshyn.³³

It is now considered unlikely that the findings in $d(\gamma,p)n$ force us to modify current NN potentials, and speculations concerning the influence of the six-quark nature of the deuteron at small separation distances³⁴ seem, at least, premature. However, it seems clear that, as our understanding of the $d(\gamma,p)n$ process improves, eventually

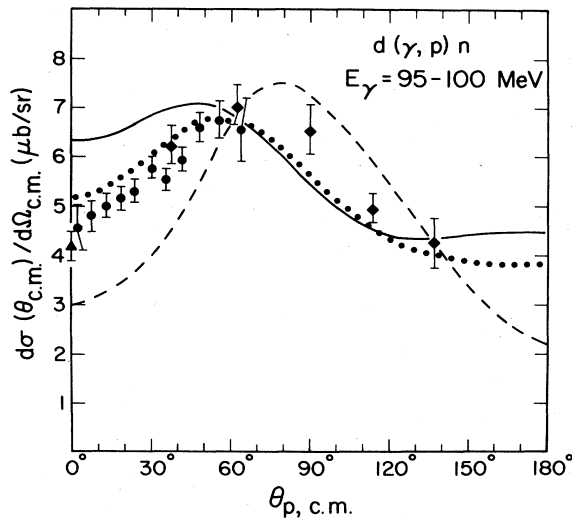


FIG. 6. The results of this experiment, converted to the $d(\gamma,p)n$ framework, are shown as solid circles. The triangle has been obtained from the Main data (Ref. 6) by interpolation. The diamonds are the most recent data from photodisintegration (Ref. 22). The solid curve shows Partovi's calculation (Ref. 4) based on the Hamada-Johnston potential. If the Lomon-Feshbach NN interaction with $P_D=4.6\%$ is used instead, the dotted curve is obtained (Ref. 32). Hwang's elementary particle treatment yields the dashed curve (Ref. 43). The dotted curve is calculated with $E_\gamma=95$ MeV, the other two curves with $E_\gamma=100$ MeV.

the role of the NN interaction has to be critically evaluated.

The importance of contributions from the exchange of mesons and the presence of intermediate isobars was demonstrated for $n+p$ capture at thermal energies.³⁵ At higher energies, such exchange currents were studied by Miller and Arenhövel³⁶ and a number of theoretical groups thereafter (see Refs. 37 and 38 and references therein).

Meson exchange currents are important; they are also contained implicitly in most calculations carried out so far, since the commonly used Siegert operator³⁹ generates some contribution of two-body currents even if the two-body charge density is neglected. In Fig. 7, the dash-dot curve shows a classical impulse approximation calculation³⁷ where the Siegert operator is the *only* source of two-body effects. This curve is identical with Partovi's result.⁴ If additional explicit exchange effects are taken into account, the dashed line is obtained.³⁷ The Siegert operator accounts for most of the exchange contributions, as is seen from an impulse approximation calculation³⁷ without it (dotted curve).

Recently, the roles of relativity and corresponding higher-order corrections to the charge density have been studied.^{31,40,41} The effect on the two-body charge density is small,⁴² but sizable contributions arise from relativistic corrections of the one-body charge density through the so-called Darwin-Foldy and spin-orbit terms.⁴¹ Calculations depend sensitively on the π NN coupling scheme: At present pseudovector coupling seems to lead to better agreement with the data. The effect of such corrections is

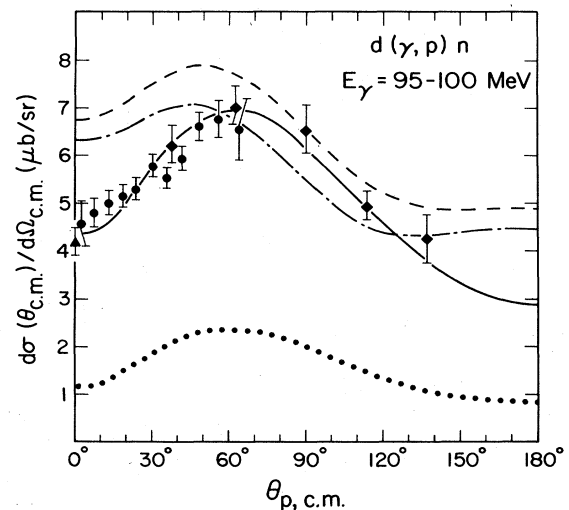


FIG. 7. The data are the same as in Fig. 6. Three calculations from Ref. 37 illustrate meson exchange contributions (MEC's): the dash-dot curve contains MEC's implicitly through the use of Siegert's operator [same as Partovi's result (Ref. 4), solid curve Fig. 6]; in the dotted curve all MEC's are excluded, and the dashed curve contains additional, explicit MEC's. The solid curve illustrates the effect of one- and two-body relativistic corrections (Refs. 40 and 41) in pseudovector coupling; it has been obtained from Ref. 22.

illustrated in Fig. 5, where the difference between shaded and stippled regions is caused by the inclusion of relativistic effects in the $E1$ transition operator.³¹ A similar result was obtained by the Florence group.^{40,41} An angular distribution of the cross section where relativistic contributions to the one- and two-body density in pseudovector coupling were taken into account^{40,41} is shown as a solid curve in Fig. 7. As can be seen, this theoretical approach is consistent with the data over essentially the whole angular region, and thus removes the longstanding discrepancy. Although the agreement with the data is suggestive, it is important to realize that these "relativistic" calculations only discuss *corrections* to the transition operator but neglect relativity in the wave functions, and thus are internally inconsistent.

An independent approach towards understanding deuteron photodisintegration was presented by Hwang⁴³ *et al.* in their so-called elementary particle treatment.⁴³ This model differs from Partovi's model in the method by which gauge invariance is enforced, in a different choice of reference frame, and in the inclusion of higher multipole terms. The calculated cross sections (dashed curves in Figs. 5 and 6) are, however, in serious disagreement with the data.

An expansion of the reaction amplitude into leading diagrams has been used by Laget.⁴⁴ Recently, the continuum state interaction, which was previously limited to s waves, was expanded to include p waves which resulted in a large effect (20% at forward angles) on the $E_\gamma = 100$ MeV cross section.⁴⁵

The principal difficulty one faces in trying to compare the various theoretical treatments is in attempting to assess how the calculations differ from each other in their physical content, rather than in their calculational approach.

V. CONCLUSIONS

We have presented measurements of the differential cross section for the $p(n,d)\gamma$ reaction at center-of-mass angles between 0° and 65° at a neutron kinetic energy of $T_n = 185$ MeV. In this experiment the *ratio* between the

capture cross section and the cross section for neutron-proton elastic scattering was determined, a method which makes our result insensitive to many systematic uncertainties. Our $p(n,d)\gamma$ cross section depends directly on the values adopted for the $p(n,p)n$ cross section. Because existing data and phase shift parametrizations of neutron-proton scattering at 200 MeV show inconsistencies at the level of $\pm 8\%$, as outlined in Sec. III A, the data in this paper are presented in such a way that a reevaluation in light of better values for the $p + n$ elastic cross section is easily possible.

At $\theta = 0^\circ$ our measurement agrees, within errors, with the photodisintegration data from Mainz.⁶ Comparison with other data sets is made in Sec. III B.

Among the various theoretical treatments of radiative transitions in the NN system, those involving relativistic corrections are at present the most consistent with our measurements. This supports the mounting suspicion that the disparity between theory and experiment cannot be resolved by either manipulating the underlying NN interaction, or by explicitly including meson exchange contributions, but that there is need for a careful study of the relativistic aspects of this process. This will have to be done with as much internal consistency as possible.

It has become clear that measurements at $\theta = 0^\circ$ may not play an exclusive role in evaluating competing theoretical efforts, but that reliable cross section information at all angles up to 180° is of crucial importance. We have also neglected to mention polarization observables, although it is obvious that medium-energy radiative capture experiments with polarized beam and/or target are becoming feasible⁴⁶ and will be needed for a better understanding of this fundamental process of nuclear physics.

ACKNOWLEDGMENTS

The authors would like to express their thanks to K. Komisarck and W. Estrada for help in operating the cryotarget. The research presented here was supported by a grant from the National Science Foundation (No. PHY 81-14339).

¹J. Chadwick and M. Goldhaber, *Nature* **134**, 237 (1934).

²H. A. Bethe and R. E. Peierls, *Proc. R. Soc. (London) Ser. A* **148**, 146 (1935).

³G. Breit and E. U. Condon, *Phys. Rev.* **49**, 904 (1936).

⁴F. Partovi, *Ann. Phys. (N.Y.)* **27**, 79 (1964).

⁵B. Weissmann and H. Schultz, *Nucl. Phys.* **A174**, 129 (1971).

⁶R. J. Hughes, A. Zieger, H. Wäffler, and B. Ziegler, *Nucl. Phys.* **A276**, 329 (1967).

⁷F. W. K. Firk, in *Proceedings of the 3rd International Symposium on Neutron Capture Gamma-ray Spectroscopy and Related Topics*, edited by R. E. Chrien and W. R. Kane (Plenum, New York, 1979).

⁸J. F. Gilot, A. Bol, P. Leleux, P. Lipnik, and P. Macq, *Phys. Rev. Lett.* **47**, 304 (1981).

⁹H. O. Meyer, J. R. Hall, M. Hugi, H. J. Karwowski, R. E. Pollock, and P. Schwandt, *Phys. Rev. Lett.* **52**, 1759 (1984).

¹⁰K. Komisarck, H. O. Meyer, T. Bertuccio, W. Manwaring, and W. Smith, Indiana University Cyclotron Facility IUCF report, 1984.

¹¹J. Källne and B. Fagerström, University of Uppsala, Gustav Werner Institute Internal Report GWI-PH3/75, 1975.

¹²J. C. Allred, A. H. Armstrong, and L. Rosen, *Phys. Rev.* **91**, 90 (1953).

¹³Yu. M. Kazarinov and Yu. N. Simonov, *Zh. Eksp. Teor. Fiz.* **33**, 614 (1957) [*Sov. Phys.—JETP* **16**, 24 (1963)].

¹⁴B. E. Bonner, J. E. Simmons, C. L. Hollas, C. R. Newsom, P. J. Riley, G. Glass, and M. Jain, *Phys. Rev. Lett.* **41**, 1200 (1978).

¹⁵R. A. Arndt, L. D. Roper, R. A. Bryan, R. B. Clark, B. J. VerWest, and P. Signell, *Phys. Rev. D* **28**, 97 (1983).

¹⁶M. Lacombe, B. Loiseau, J. M. Richard, and R. Vinh Mau, *Phys. Rev. C* **21**, 861 (1980).

- ¹⁷E. A. Whalin, B. D. Schrieffer, and A. O. Hansen, *Phys. Rev.* **101**, 377 (1956).
- ¹⁸J. C. Keck and A. V. Tollestrup, *Phys. Rev.* **101**, 360 (1956).
- ¹⁹Iu. A. Aleksandrov, N. B. Delone, L. I. Slovokhotov, G. A. Sokol, and L. N. Shtarkov, *Zh. Eksp. Teor. Fiz.* **43**, 35 (1962) [*Sov. Phys.—JETP* **6**, 472 (1958)].
- ²⁰R. Kose, W. Paul, and K. Stockhorst, *Z. Phys.* **202**, 364 (1967).
- ²¹P. Dougan, V. Ramsay, and W. Stiefner, *Z. Phys. A* **280**, 341 (1977).
- ²²G. P. Capitani, E. DeSanctis, P. DiGiacomo, C. Guaraldo, V. Lucherini, E. Polli, A. R. Reolon, and R. Scrimaglio, in *Proceedings of the Workshop on Perspectives in Nuclear Physics at Intermediate Energies*, edited by S. Boffi, C. Ciofi, and M. M. Giannini (World Scientific, Singapore, 1984).
- ²³J. Matthews, private communication.
- ²⁴D. A. Hutcheon, private communication.
- ²⁵G. Nicklas, J. Franz, E. Rossle, and H. Schmitt, *Phys. Lett.* **141B**, 170 (1984).
- ²⁶S. Barshay, *Phys. Rev. Lett.* **17**, 49 (1966).
- ²⁷D. F. Bartlett, C. E. Friedberg, P. E. Goldhagen, and K. Goulianos, *Phys. Rev. Lett.* **27**, 881 (1971).
- ²⁸M. L. Rustgi, T. S. Sandhu, and O. P. Rustgi, *Phys. Lett.* **70B**, 145 (1977); E. L. Lomon, *ibid.* **68B**, 419 (1977).
- ²⁹E. L. Lomon, *Phys. Lett.* **68B**, 491 (1977).
- ³⁰M. E. Schulze, D. P. Saylor, and R. Goloskie, *Phys. Rev. C* **24**, 2435 (1981).
- ³¹J. L. Friar, in *Proceedings of the Workshop on Perspectives on Nuclear Physics at Intermediate Energies*, edited by S. Boffi, C. Ciofi, and M. M. Giannini (World Scientific, Singapore, 1984).
- ³²E. L. Lomon and H. Feshbach, *Ann. Phys. (N.Y.)* **48**, 94 (1968).
- ³³J. M. Greben and R. M. Woloshyn, *J. Phys. G* **9**, 643 (1983).
- ³⁴E. Hadjimichael and D. P. Saylor, *Phys. Rev. Lett.* **45**, 1776 (1980).
- ³⁵D. O. Riska and G. E. Brown, *Phys. Lett.* **38B**, 193 (1972).
- ³⁶H. G. Miller and H. Arenhövel, *Phys. Rev. C* **7**, 1003 (1973).
- ³⁷H. Arenhövel, *Nuovo Cimento* **76A**, 256 (1983).
- ³⁸M. L. Rustgi, R. Vyas, and O. P. Rustgi, *Phys. Rev. C* **29**, 785 (1984).
- ³⁹E. Hadjimichael, *Phys. Lett.* **85B**, 17 (1979).
- ⁴⁰A. Cambi, B. Mosconi, and P. Ricci, *Phys. Rev. Lett.* **48**, 462 (1982).
- ⁴¹A. Cambi, B. Mosconi, and P. Ricci, *J. Phys. G* **10**, L11 (1984).
- ⁴²W. Jaus and W. S. Woolcock, *Nucl. Phys.* **A365**, 477 (1981).
- ⁴³W.-Y.P. Hwang, J. T. Londergan, and G. E. Walker, *Ann. Phys. (N.Y.)* **149**, 335 (1983).
- ⁴⁴J. M. Laget, *Nucl. Phys.* **A312**, 265 (1978).
- ⁴⁵J. M. Laget, private communication.
- ⁴⁶J. M. Cameron, C. A. Davis, H. Fielding, P. Kitching, J. Soukup, J. Uegaki, J. Wesick, H. S. Wilson, R. Abegg, D. A. Hutcheon, C. A. Miller, A. W. Stetz, Y. M. Shin, N. Stevenson, and I. J. van Heerden, *Phys. Lett.* **137B**, 315 (1984).